Input Impedance Analyses of Charge Controlled and Frequency Controlled LLC Resonant Converter

Suyash Sushilkumar Shah
Electrical & Computer Engineering
North Carolina State University
Email: sshah7@ncsu.edu

Utkarsh Raheja
Electrical & Computer Engineering
North Carolina State University
Email: utkarsh335@gmail.com

Subhashish Bhattacharya
Electrical & Computer Engineering
North Carolina State University
Email: sbhatta4@ncsu.edu

***Abstract*—LLC resonant converters are popular for point-of-load *dc-dc* conversion in applications such as data-centers and electric vehicles. In complex systems, where converters are cascaded to feed disparate loads, system stability issues related to the impedance interaction in converters may arise. At the very least, the designed system must satisfy Middlebrook's criterion for stable operation; therefore, the knowledge of input and output impedance of converters is essential. In this respect, the paper analyses the impact of two control strategies of LLC resonant converter on its input impedance. The two strategies are: conventional variable frequency control (VFC) and bang-bang charge control (BBCC). The input impedance models of LLC resonant converter in case of these two strategies are derived. The developed models are validated through impedance plots extracted from simulation. Further, the models are applied to a system comprising of a dual active bridge (DAB) converter feeding a single LLC resonant point-of-load converter to investigate the impact of two strategies on the stability of such cascaded systems.**

***Keywords*—Bidirectional dc-dc converter, LLC resonant converter, frequency control, charge control, input impedance, stability, cascaded system.**

I. Introduction

Power electronic applications in data-centres and heavy-duty vehicles convert voltages of greater than 400V sourced from transmission lines or on-board generator sets to local load voltages of less than 60V. Since the power requirement of a single load converter is much lower than that of the complete system, a distributed power system (DPS) is typically preferred [1], [2]. It consists of a high-power central converter feeding multiple low-power point-of-load (POL) converters. The modular structure of the architecture allows reduced cabling costs, heat distribution, improved system availability, better transient response and flexibility of modification. In such systems, however, the interaction of output impedance of the source converter with the input impedance of POL converters can cause unstable oscillations at the intermediate *dc* bus [3], [4]; hence, system stability forms an important design parameter.

A typical requirement of POL converters in automotive or data-centre applications is to operate with nominally varying input voltage and wide load-variation. Hence, LLC resonant converters, which are capable of soft-switching for the entire load and input voltage range resulting in high operational efficiency and reduced electromagnetic interference (EMI), [5] have become a preferred choice. The converter is typically controlled by modulating the switching frequency of the primary side bridge. It is called as variable frequency control (VFC). It is designed to, nominally, operate at and about its series resonant frequency. In this strategy, depending on its operating point, a double-pole resonance is observed in its uncompensated loop gain [6]. It appears due to resonance between the equivalent resonant inductance, as defined in [6], and the output filter capacitor; its amplitude is load dependent.

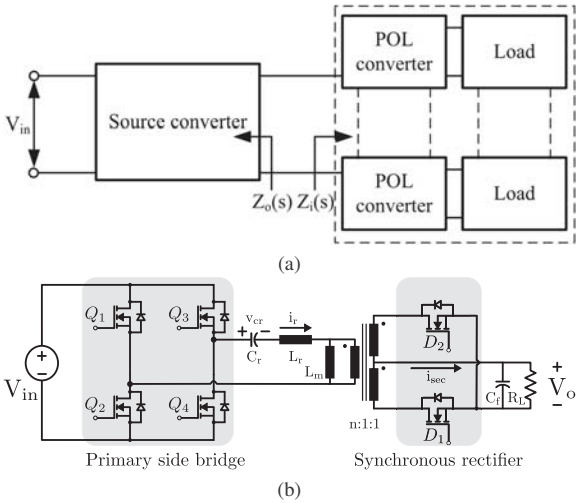

Fig. 1: (a) Typical configuration of distributed power system, (b) LLC resonant converter schematic for POL applications.

Many methods to model the VFC-based resonant conversion systems have been developed. In [7], the principles of amplitude modulation (AM) and frequency modulation (FM) are utilized to model the envelope dynamics of such systems. A generalized averaging approach is described in [8], which uses time-dependent Fourier series expansion of *ac* quantities. A phasor transformation approach [9] and sampled-data system approach [10] were also proposed for such systems. In this paper, extended describing function (EDF) method [11] is utilized to model the VFC-based LLC resonant converter.

Another strategy to control the LLC resonant converter is bang-bang charge control (BBCC), recently developed for half-bridge topology in [12]. The resonant capacitor voltage is measured and compared against a threshold which determines the switching instants. It is similar to hysteresis current control strategy employed in PWM converters [13]; the control variable is the resonant capacitor voltage threshold. It allows elimination of the double-pole resonance observed in VFC and

TABLE I: System parameters

Parameter	Variable	Value
Input voltage	V_{in}	270 V
Output voltage	V_o	28 V
Series capacitor	C_r	29 nF
Series inductor	L_r	26 μH
Magnetizing inductor	L_m	95 μH
Resonant frequency	f_o	185 kHz
Turns-ratio	n	10
Output capacitance	C_f	750 μF

has a first-order transient response, permitting high control bandwidth of up to one-sixth of the switching frequency.

The control-to-output transfer function is modified from a second order system in VFC-based LLC resonant converter to a first order system in BBCC-based converter. In addition, the perturbation in the input voltage affects a disparate response in the input current, indicating that the input impedance in the two cases is different. The objective of the paper is to derive analytic expressions of the input impedance of LLC resonant converter for VFC and BBCC control methods. Further, the impact of these strategies on the stability margins of a cascaded converter system is studied using the developed models.

Some authors have presented the input impedance of VFC-based LLC converter in [14], [15]. In the present case, the input impedance is derived for the VFC-based LLC converter using the model developed in [6]. Further, the closed-loop input impedance model of BBCC-based full-bridge LLC converter is also developed. The small-signal model of full-bridge LLC resonant converter operating with BBCC strategy is extended from the concept reported in [12] a priori. Subsequently, the impact of the two strategies on the stability of cascaded systems is illustrated through an example where a central dual active bridge (DAB) converter feeds a single LLC resonant converter.

The paper is organized as follows: in section II, the input impedance characteristics of VFC-based LLC converter are analyzed for a sample system design. Section III derives the control model for BBCC-based full-bridge LLC resonant converter before developing the model for its input impedance characteristics. Further, the two models are validated through simulation. Finally, the two strategies are compared by way of cascading the converter with a dual active bridge (DAB) based source converter in section IV. The results from circuit simulation are used to validate the developed analyses. The parameters of the system, including those of the resonant circuit, used to illustrate the difference between the input impedance of the LLC resonant converter operating in VFC or BBCC strategy are listed in Table I.

II. Impedance Analysis: Frequency Control

The conventional control strategy used for LLC resonant converters varies the frequency of the voltage applied to the resonant tank to modulate its gain. This is referred to in the paper as variable frequency control (VFC) and its schematic is shown in Fig. 2. Several papers report the small-signal model of the converter using various methods, including the popular extended describing function (EDF) method [11].

A unified third-order small-signal equivalent model [6], shown in Fig. 3, is used to calculate the input impedance of

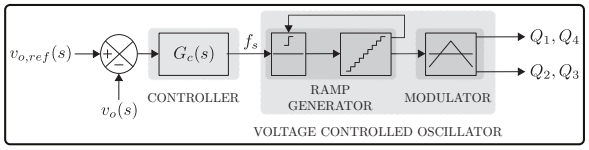

Fig. 2: Schematic of variable frequency control strategy.

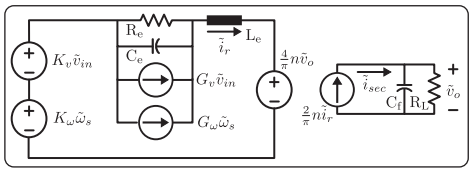

Fig. 3: Unified model of LLC converter illustrated in [6].

the converter. The parameters of the control model across the operating range of the LLC converter are given in [6] and recounted here in (1).

$$L_e = \begin{cases} L_r(1+\dfrac{1}{\omega_n^2}), & \text{if } \omega_n \geq 1 \\ L_r(1+\dfrac{1}{\omega_n^2}) + L_m(1-\omega_n), & \text{if } \omega_n < 1 \end{cases}$$
$$R_e = \begin{cases} \dfrac{\omega_o L_e |X_{eq}||\omega_n - 1|}{R_{eq}}, & \text{if } \omega_n \geq 1 \\ 0, & \text{if } \omega_n < 1 \end{cases} \quad (1)$$
$$R_{eq} = \frac{8}{\pi^2}n^2 R_L \; ; \; X_{eq} = \omega_s L_r - \frac{1}{\omega_s C_r} \; ; \; \omega_n = \frac{\omega_s}{\omega_o}$$

A typical LLC resonant converter is designed to nominally operate at or close to series resonant frequency, ω_o. Additionally, a switching frequency less than the resonant frequency is preferred due to zero-current switching (ZCS) of the secondary side semiconductor devices. In any case, for operation close to and at the series resonant frequency, the equivalent small-signal circuit resistance (R_e) nearly equals zero, i.e. the corresponding branch in the small-signal equivalent circuit model of Fig. 3 is shorted. Therefore, a double-pole resonance between the equivalent small-signal circuit inductance (L_e) and the reflected, primary-referred output capacitance, $(\pi^2/8)(C_f/n^2)$ is observed in all its

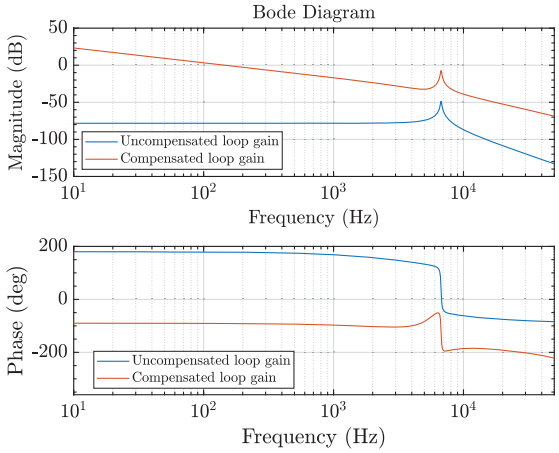

Fig. 4: Uncompensated and compensated loop gains of LLC converter with VFC strategy.

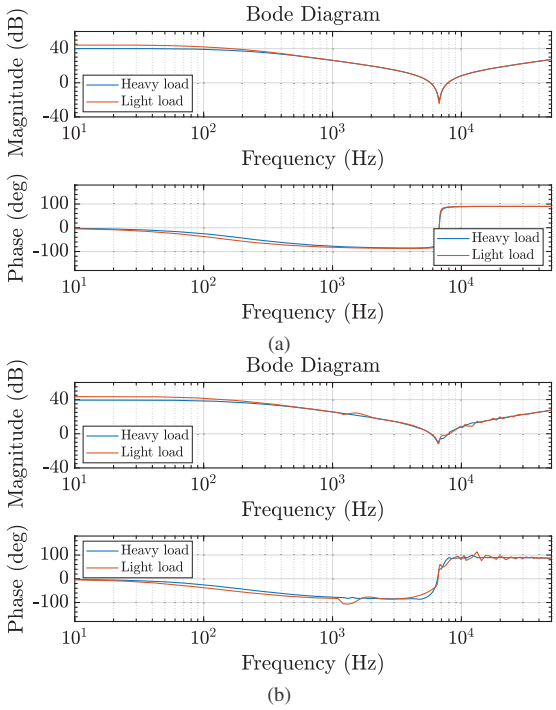

Fig. 5: Open-loop input impedance plots derived from (a) analytic model and (b) simulation for heavy and light load for VFC-based LLC resonant converter.

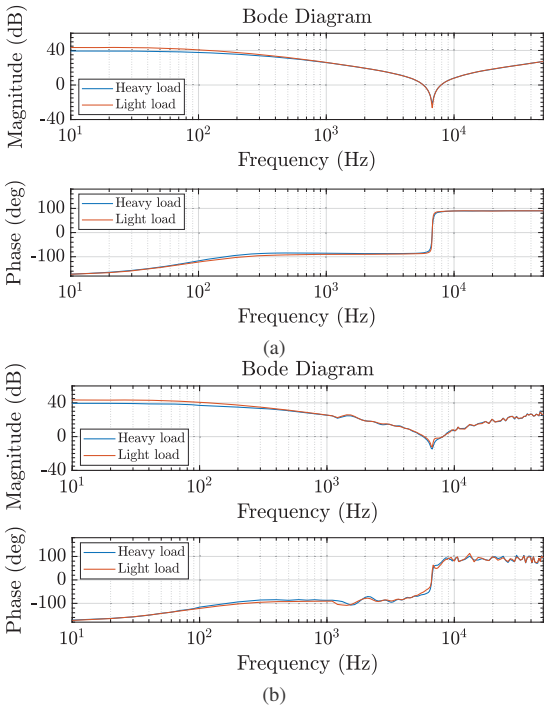

Fig. 6: Closed-loop input impedance plots derived from (a) analytic model and (b) simulation for heavy and light load for VFC-based LLC resonant converter.

transfer functions. From Fig. 3, the expression of plant transfer function of VFC-based LLC resonant converter may be derived as in (2).

$$\frac{\tilde{v}_s(s)}{\tilde{f}_s(s)} = \frac{4n \cdot K_\omega \cdot R_L}{s^2 \cdot (L_e C_f R_L) + s \cdot L_e + R_{eq}} \tag{2}$$

The impedance models developed in this section are validated through a 1kW, 270V/28V LLC resonant converter system. The other system parameters are listed in Table I. The double pole appearing in the uncompensated loop gain plot at the frequency determined by L_e and C_f reduces the phase-margin of the closed-loop system. It indicates that a simple PI regulator may not be sufficient to satisfactorily control the converter system. Therefore, a controller, given in (3), is designed so that the double pole resonance appears after the cross-over frequency of the compensated system. The uncompensated and compensated loop gain plots are illustrated in Fig. 4.

$$G_c(s) = \frac{s^2 \cdot (-54.675 \cdot 10^{-4}) - s \cdot 105 - 750 \cdot 10^4}{s^3 \cdot (2.56 \cdot 10^{-12}) + s^2 \cdot (2.3 \cdot 10^{-6}) + s} \tag{3}$$

A. Input impedance analysis

The impedance of the VFC-based LLC resonant converter may be derived from its small-signal equivalent circuit in Fig. 3. The impedance of the resonant tank, as seen from the input-side, is calculated by forcing the perturbation in control variable, $\tilde{\omega}_s$, to zero. Subsequently, the impedance at the *dc* input of the converter is derived by reflecting the resonant tank current, i_r, to the input-side *dc* current, i_{in}, using (4).

$$\tilde{i}_{in}(s) = \frac{2}{\pi}\tilde{i}_r(s) \tag{4}$$

$\tilde{i}_{in}$ and $\tilde{i}_r$ are the perturbations in input current and resonant tank current, respectively. Solving for $\tilde{i}_{in}$ in terms of $\tilde{v}_{in}$, the open-loop input impedance of the converter in VFC strategy is expressed in (5).

$$\frac{1}{Z_D(s)} = \frac{2}{\pi}\frac{s \cdot C_f R_L + 1}{s^2 \cdot (L_e C_f R_L) + s \cdot L_e + R_{eq}} \tag{5}$$

The open-loop input impedance of VFC-based LLC resonant converter is plotted for the given system parameters, in Fig. 5a. Two load conditions ($R_L = 1\Omega$ and $R_L = 1.6\Omega$) have been considered. *PLECS v4.1.8* is used to validate the developed input impedance model by appropriate placement of perturbation sources and response observers in the circuit simulation model; the extracted input impedance plots are shown in Fig. 5b. It is evident that the developed model of the converter agrees with that extracted from simulation. The double pole predicted by the model is also apparent in these plots. Note that in light load condition, the peak of the double pole resonance is sharper and larger indicating that the system may be more prone to instability in these conditions. The deviation in magnitude at the double pole resonant frequency between simulation results and the model appears due to inadequate resolution of the frequency sweep.

Any converter system is rarely operated in open loop. Therefore, it is imperative to derive its closed-loop input impedance for stability analyses. The closed-loop input impedance of any converter has two components [16]. It can be expressed in terms of loop gain, $T(s)$, as shown in (6).

$$\frac{1}{Z_{iCL(\text{VFC})}(s)} = \frac{1}{Z_N(s)}\frac{T(s)}{1+T(s)} + \frac{1}{Z_D(s)}\frac{1}{1+T(s)} \quad \text{where, } \frac{1}{Z_N(s)} = -\frac{I_{in}}{V_{in}} \tag{6}$$

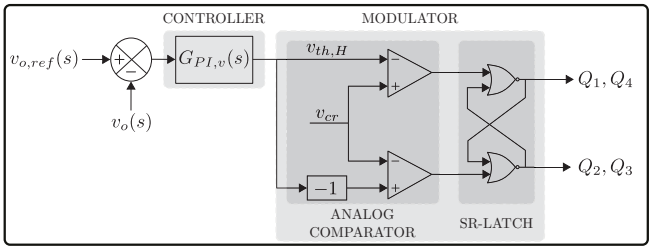

Fig. 7: Schematic of bang-bang charge control strategy.

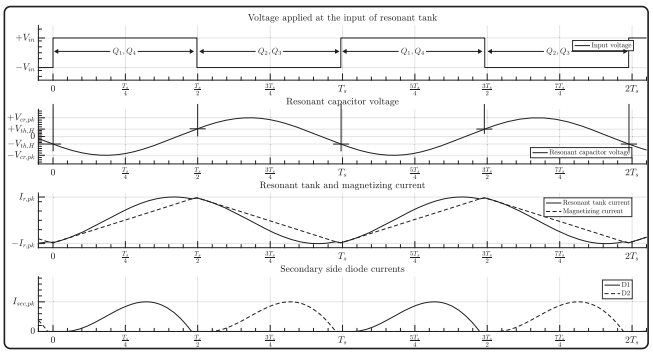

Fig. 8: Typical waveforms for bang-bang charge control.

V_{in} and I_{in} are the nominal steady-state values of the input voltage and current, respectively. For low frequencies, well within the control loop bandwidth, the converter feeding a resistive load behaves like a constant power load. It indicates a negative resistance, Z_N, at its input terminals. It is also observed in the closed-loop input impedance plot in Fig. 6a that its low frequency response has a phase of -180°. The open-loop input impedance, Z_D, dominates beyond the control bandwidth, whereby a resonance between the equivalent small-signal model inductance, L_e, and the reflected, primary-referred output capacitance, $(\pi^2/8)(C_f/n^2)$, is observed in Fig. 6a. The closed-loop impedance plots are also extracted from simulation and shown in Fig. 6b. The developed low frequency model agrees with the simulation results.

III. Impedance analysis: Charge control

In this section, the charge control method developed in [2] for a half-bridge LLC converter is extended to full-bridge LLC resonant converter. The charge-control method is explained through Fig. 7 and Fig. 8. The modulator shown in Fig. 7 compares the measured resonant capacitor voltage, V_{cr}, with a threshold, $V_{th,H}$. When the capacitor voltage exceeds the negative threshold, $-V_{th,H}$, the semiconductor devices Q_2, Q_3 are turned off and complementary switches Q_1, Q_4 are turned on. The input voltage to the resonant circuit switches from V_{in} to $+V_{in}$. The negative current in the series resonant inductor, L_r, transfers the energy from the inductor into the resonant capacitor, C_r, thereby increasing the capacitor voltage in the negative direction. When the inductor current falls to zero, the capacitor voltage reaches its negative-peak and begins to rise. The behavior of the resonant circuit depends on the load connected at the converter output. The capacitor voltage continues to rise, until it crosses the positive threshold, $+V_{th,H}$, when devices Q_1, Q_4 are turned off and Q_2, Q_3 are turned on.

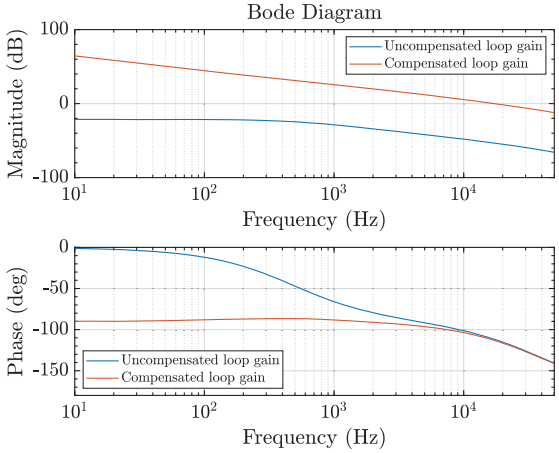

Fig. 9: Uncompensated and compensated loop gains of LLC converter with BBCC strategy.

The change in the resonant capacitor voltage over one switching cycle is indicative of the average input charge (Q_{net}) drawn from the supply during the time when devices Q_1, Q_4 are turned-on, i.e. when the input voltage to the resonant circuit is $+V_{in}$. The product of the capacitor value and the total change in its voltage in the half-cycle, from $-V_{th,H}$ to $+V_{th,H}$, is amount of charge transferred during the half-cycle. Therefore, the total energy drawn from the supply in one switching cycle can be expressed as in (7). In steady-state, where all parameters including the switching frequency, f_s, are constant, the power transmitted through the converter can be expressed by P_{net}. It is clear from (7) that any change in input voltage, resonant capacitor threshold voltage or transmitted power affects a change in the switching frequency, f_s.

$$\begin{aligned} P_{net} &= V_o I_{sec} = V_{in} I_{in} = V_{in} \cdot Q_{net} \cdot (2f_s) \\ &= 4 \cdot V_{in} \cdot C_r \cdot f_s \cdot V_{th,H} \end{aligned} \tag{7}$$

Assuming a loss-less conversion, the output power may be regulated by controlling the threshold voltage of the resonant capacitor at which the switching decisions are made. The small-signal model for full-bridge LLC resonant converter is developed by the method described in [12]. The average *dc* output current, i_{sec}, calculated from (7) is described in (8).

$$i_{sec} = \frac{P_{net}}{V_o} = \frac{4 \cdot V_{in} \cdot C_r \cdot f_s \cdot V_{th,H}}{V_o} \tag{8}$$

The small-signal perturbation in average output current, $\tilde{i}_{sec}$, is expressed in terms of perturbations in output voltage, input voltage, resonant capacitor voltage threshold and switching frequency (9). For computing the control to output transfer function, the perturbation in input voltage is forced to zero. The switching frequency perturbation is eliminated from the equation by using its small-signal relationship with the output voltage perturbation.

$$\begin{aligned} \tilde{i}_{sec}(s) =& K_a \tilde{v}_o(s) + K_b \tilde{v}_{th,H}(s) + K_c \tilde{f}_s(s) + K_e \tilde{v}_{in}(s) \\ =& K_a \tilde{v}_o(s) + K_b \tilde{v}_{th,H}(s) + K_c K_d \tilde{v}_o(s) + K_e \tilde{v}_{in}(s) \\ \text{where, } K_a = \frac{\partial i_{sec}}{\partial V_o} &; K_b = \frac{\partial i_{sec}}{\partial V_{th,H}} ; K_c = \frac{\partial i_{sec}}{\partial f_s} ; \\ K_d = \frac{1}{\partial V_o / \partial f_s} &\text{ and } K_e = \frac{\partial i_{sec}}{\partial V_{in}} \end{aligned} \tag{9}$$

The perturbations in the average *dc* output current are translated to perturbations in output voltage through the output filter impedance, Z_f.

$$\tilde{v}_o(s) = \tilde{i}_{sec}(s) \cdot Z_f = \tilde{i}_{sec} \cdot \frac{R_L}{sC_f \cdot R_L + 1} \tag{10}$$

The control-to-output transfer function of a BBCC-based LLC resonant converter may be derived from (9) and (10) and is expressed in (11). The approach is described in [12] and extended here for full-bridge LLC resonant converter.

$$\frac{\tilde{v}_o(s)}{\tilde{v}_{th,H}(s)} = \frac{4 \cdot V_{in} \cdot C_r \cdot f_s \cdot V_o \cdot R_L}{V_o^2(1 + sC_fR_L) - 4V_{in}C_rV_{th,H}R_L(K_dV_o - f_s)}$$

where,

$$V_o = \frac{V_{in}/n}{\sqrt{\left(1 + \gamma - \gamma(f_n)^{-2}\right)^2 + Q^2(f_n - f_n^{-1})\left(1 + (f_n)^{-2}\right)}}$$

$$Q = \frac{\pi^2}{8}\frac{1}{n^2R_L} \cdot \sqrt{\frac{L_r}{C_r}} \; ; \; f_n = \frac{f_s}{f_o} \; ;$$

$$\gamma = \frac{L_r}{L_m} \; ; \; \frac{1}{K_d} = \frac{\partial V_o}{\partial f_s} = \frac{\tilde{v}_o(s)}{\tilde{f}_s(s)} \; ; \; V_{th,H} = \frac{V_o^2}{R_L}\frac{1}{4V_{in}C_rf_s} \tag{11}$$

The factor K_d may be found by calculating the derivative of the static gain-curve at a particular operating point. The assumption is valid for perturbation frequencies much lower than the switching frequency. The uncompensated (11) and compensated loop-gains of charge-controlled LLC resonant converter, derived from (11), are plotted in Fig. 9. The first order response of the charge control method allows utilization of a simple proportional-integral (PI) controller given in (12).

$$G_{PI,v}(s) = 480\Big(1 + 2\pi\frac{410}{s}\Big) \tag{12}$$

A. Input impedance analysis

The open-loop input impedance is derived by forcing the perturbation in control variable to zero. The control variable in BBCC strategy is the resonant capacitor voltage threshold, $v_{th,H}$, Hence, to calculate the open-loop input impedance when the $\tilde{v}_{th,H}$ is forced to zero, the perturbation in the frequency, $\tilde{f}_s$, is non-zero. It is because any perturbation in the input voltage will result in different switching instants and hence, different frequency. Foremost, the steady-state average input current is directly dependent on the resonant capacitor voltage threshold, $v_{th,H}$, and switching frequency, f_s.

$$I_{in} = 4 \cdot C_r \cdot V_{th,H} \cdot f_s \tag{13}$$

Therefore, the perturbation in average input current is a function of perturbations in switching frequency and resonant capacitor voltage threshold. As aforementioned, the control variable, $\tilde{v}_{th,H}$, is forced to zero.

$$\tilde{i}_{in}(s) = 4 \cdot C_r \cdot V_{th,H} \cdot \tilde{f}_s(s) \tag{14}$$

Similarly, the perturbation in output voltage may independently be expressed in (15).

$$\tilde{v}_o(s) = \frac{\partial V_o}{\partial f_s}\tilde{f}_s(s) + \frac{\partial V_o}{\partial V_{in}}\tilde{v}_{in}(s) \tag{15}$$

At perturbation frequencies much lower than the switching frequency, (15) may be re-written as (16).

$$\tilde{v}_o(s) = \frac{1}{K_d} \cdot \tilde{f}_s(s) + \frac{V_o}{V_{in}} \cdot \tilde{v}_{in}(s) \tag{16}$$

At low perturbation frequencies, K_d is the slope of the static gain-curve as expressed in (11), relating the output voltage variations to the perturbations in switching frequency. Similarly, its dependence on input voltage may also be assumed proportional for low frequency perturbations.

In order to derive the input impedance of charge-controlled LLC resonant converter at low frequencies, (7) is perturbed and the following expression is obtained.

$$I_{in}\tilde{v}_{in}(s) + V_{in}\tilde{i}_{in}(s) = I_{sec}\tilde{v}_o(s) + V_o\tilde{i}_{sec}(s) \tag{17}$$

Replacing $\tilde{i}_{sec}$ and $\tilde{v}_o$ in terms of $\tilde{v}_{in}$ using (10) and (16), the following expression is obtained.

$$I_{in}\tilde{v}_{in}(s) + V_{in}\tilde{i}_{in}(s) = \frac{V_o}{R_L}\Big(sC_fR_L + 2\Big)\Big(\frac{1}{K_d}\tilde{f}_s(s) + \frac{V_o}{V_{in}}\tilde{v}_{in}(s)\Big) \tag{18}$$

Substituting for $\tilde{f}_s$ using (14), the open-loop input impedance is expressed in (19).

$$\frac{1}{Z_D(s)} = 4C_rV_{th,H}\frac{V_o}{V_{in}}\frac{\frac{V_o}{R_L}(sC_fR_L + 1)}{4C_rV_{th,H}V_{in} - \frac{1}{K_d}\frac{V_o}{R_L}(sC_fR_L + 2)} \tag{19}$$

The open-loop impedance plots derived from analyses and those extracted from simulation are illustrated in Fig. 10a and Fig. 10b, respectively. The simulation results agree well with the impedance model of the charge-controlled LLC converter.

As aforementioned, the closed-loop input impedance of a converter system is essential in analysing its stability in a system. Its expression for a charge-controlled LLC converter is found in a manner similar to that used for VFC strategy in the previous section. $T(s)$ is the compensated loop gain of the system.

$$\frac{1}{Z_{iCL(\text{BBCC})}(s)} = \frac{1}{Z_N(s)}\frac{T(s)}{1 + T(s)} + \frac{1}{Z_D(s)}\frac{1}{1 + T(s)}$$
$$\text{where, } \frac{1}{Z_N(s)} = -\frac{I_{in}}{V_{in}} \tag{20}$$

The closed-loop input impedance of BBCC-based LLC resonant converter derived from analyses is plotted in Fig. 11a. It is also extracted from simulation and results are plotted in Fig. 11b. The model agrees well with the simulation results.

It is essential to note that the above expression of input impedance model for BBCC-based LLC resonant converter is only valid for perturbation frequencies much lower than the switching frequency. For frequencies closer to switching frequency, a different analysis approach is needed and is out of scope of this paper.

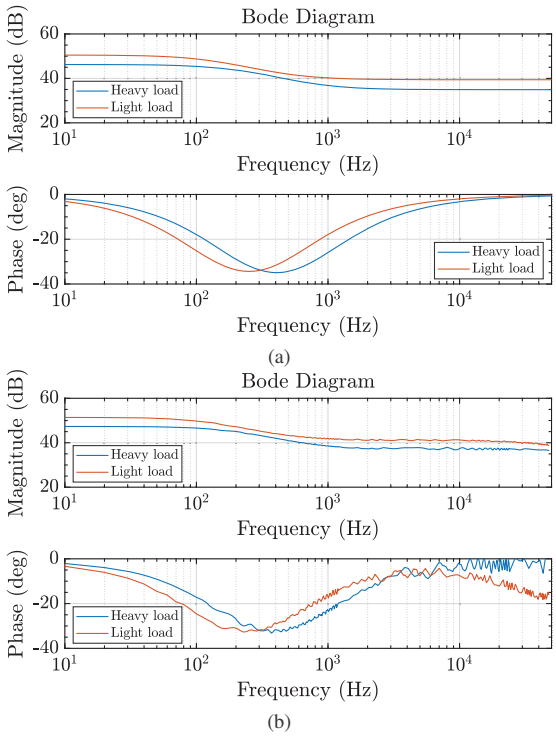

Fig. 10: Open-loop input impedance plots derived from (a) analytic model and (b) simulation for heavy and light load for BBCC-based LLC resonant converter.

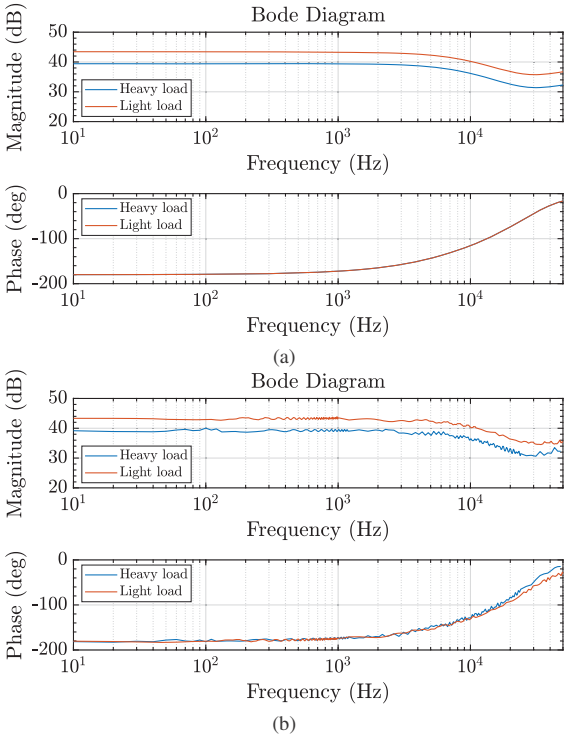

Fig. 11: Closed-loop input impedance plots derived from (a) analytic model and (b) simulation for heavy and light load for BBCC-based LLC resonant converter.

TABLE II: System parameters for DAB

Parameter	Value
Rated power	6 kW
Input voltage	500 V
Output voltage	270 V
Turns ratio	1.85:1
Inductance	9.6 µH
Output capacitor ($C_{o,\text{DAB}}$)	45 µF
Frequency	50 kHz

IV. Impact on Cascaded Converter Systems

In this section, the impact of the two control strategies of the LLC resonant converter on the stability margins of a cascaded system is studied. It is illustrated through a system comprising of a single-phase DAB converter feeding into an LLC resonant converter, as shown in Fig. 12. The DAB converter is designed according to the parameters listed in Table II. The load resistance, R_L, at the output terminals of the load converter is fixed at 1.6Ω.

In the present case, Middlebrook's stability criteria [17], which was developed for feedback controlled converter systems with input filters, is utilized to investigate the system stability. It states that if the source and load converters are independently stable, the cascaded system will be stable if,

- the magnitude of the output impedance of the source converter is less than the input impedance of the load converter for all frequencies, i.e. $Z_{o,source} < Z_{in,load}$ or,
- the phase-margin of the ratio of output impedance of the source converter to the input impedance of the load converter is positive; i.e. $\angle(Z_{o,source}/Z_{in,load}) > 0$.

Note that $Z_{o,source}$ is the output impedance of the source converter, measured when its terminals are open; and, $Z_{in,load}$ is the input impedance of the load converter measured when connected to an ideal source.

A. Minor loop gain

Any voltage source power converter can be represented by its Thévenin equivalent circuit, characterized by its Thévenin source, V_{th}, and Thévenin impedance, Z_o. The Thévenin source can be represented as a product of input voltage and a transfer function, H. The load converter presents an impedance, Z_{in}, at the output terminals of the source converter. The cascaded converter system under consideration and its Thévenin equivalent models are shown in Fig. 12. The intermediate *dc* bus voltage is, therefore, expressed by (21).

$$V_o(s) = H_1(s)V_{in}(s)\frac{1}{1+\frac{Z_{o,source}(s)}{Z_{in,load}(s)}} \tag{21}$$

Similarly, the load converter feeding a constant resistive load, $Z_L = R_L$, will generate an output voltage expressed by (22).

$$\begin{aligned} V_{o,load}(s) &= H_2(s)V_o(s)\frac{1}{1+\frac{Z_{o,load}(s)}{Z_L(s)}} \\ &= H_1(s)H_2(s)V_{in}(s)\frac{1}{1+\frac{Z_{o,source}(s)}{Z_{in,load}(s)}}\frac{1}{1+\frac{Z_{o,load}(s)}{Z_L(s)}} \\ &= \left(H_1(s)H_2(s)V_{in}(s)\frac{1}{1+\frac{Z_{o,load}(s)}{Z_L(s)}}\right)\cdot\frac{1}{1+T_m(s)} \end{aligned} \tag{22}$$

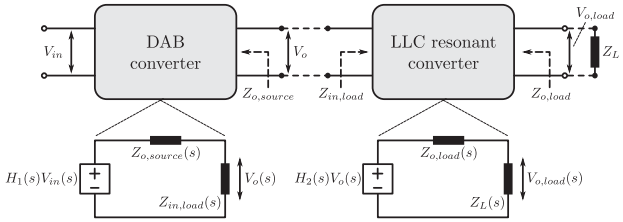

Fig. 12: Block diagram and Thévenin equivalent circuit of cascaded converter system with source and load impedances marked.

The Middlebrook stability criterion requires that the source and load converters are independently stable. Therefore, the transfer functions, $H_1(s)$ and $H_2(s)$, do not have any right half-plane poles. It also denotes that the load impedance, $Z_L(s)$, and output impedance of load converter, $Z_{o,load}(s)$, adhere to the Middlebrook criterion. Therefore, the stability of the cascaded system depends solely on the transfer function ratio of the output impedance of source converter to the input impedance of load converter; i.e. $Z_{o,source}(s)/Z_{in,load}(s)$. This is also called as minor-loop gain, indicated by $T_m(s)$, of the cascaded system. The stability margins of the cascaded converter system may, therefore, be observed by plotting the Bode diagram of its minor-loop gain, $T_m(s)$.

B. Output impedance of DAB converter

As described in previous section, the stability of a cascaded system, such as that of Fig. 12, is directly related to the output impedance of the source converter. In this case, the output impedance of the DAB converter is expressed in terms of its output filter capacitor and its compensated loop gain [18].

$$Z_{oCL(\text{DAB})}(s) = \frac{1}{sC_{o,\text{DAB}}} \frac{1}{1 + T_{\text{DAB}}(s)} \tag{23}$$

$C_{o,\text{DAB}}$ forms the output filter of the DAB converter and $T_{\text{DAB}}(s)$ is its compensated loop gain. The output filter capacitor, $C_{o,\text{DAB}}$, also includes the capacitance connected at the input terminals of the load converter. The closed-loop output impedance of DAB converter extracted from the model and from simulation are plotted in Fig. 13.

C. Stability margins of frequency controlled and charge controlled LLC resonant converter

The input impedance of the LLC resonant converter and the output impedance of the DAB converter developed previously are used to derive the minor-loop gain of the cascaded system shown in Fig. 12. In this respect, Fig. 14 compares the Bode plots of the minor loop-gain, $T_m(s)$, obtained from simulation and analytic model. In case of VFC-based LLC converter, the minor loop-gain of the cascaded system exceeds unity about the double-pole resonant frequency, while its phase-margin approaches zero. It illustrates the interaction between the input impedance of frequency-controlled LLC converter and the output impedance of DAB converter at the double-pole resonance. The low phase-margin of the minor loop gain indicates that the system with frequency-controlled LLC converter is prone to unstable oscillations on its intermediate *dc* bus. The stability margins of the system may be improved by employing complex control structures within the source and load converter systems.

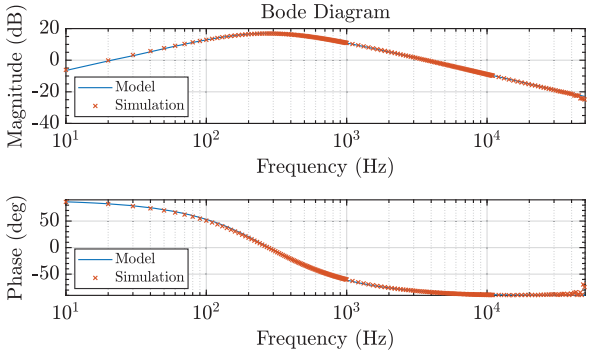

Fig. 13: Unterminated closed-loop output impedance of DAB converter extracted from the model and simulation.

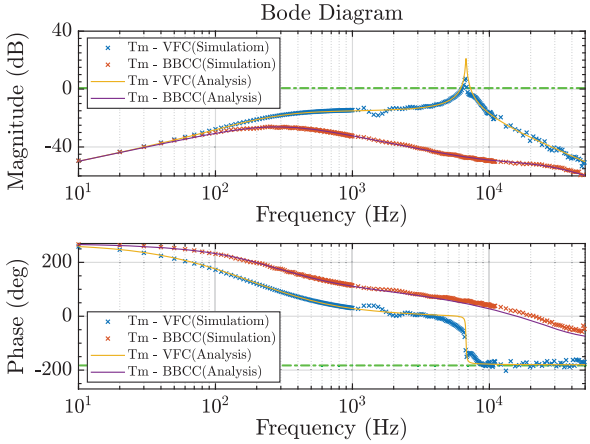

Fig. 14: Minor loop gain, $T_m(s)$, of the cascaded converter system with frequency-controlled and charge-controlled LLC converter extracted from the model and simulation.

In case of charge-controlled LLC resonant converter, the minor loop gain of the cascaded system is well within the stability margins, as marked in Fig. 14. In essence, it indicates that besides improvement in the closed-loop control bandwidth of LLC resonant converter when BBCC method is employed, the cascaded system exhibits superior stability margin.

The above analysis becomes particularly important for applications where multiple LLC resonant converters are loading a single source converter. Such applications may be found in the auxiliary power supply systems of an automotive or those of a data-center. In such cases, the input impedance of the several load converters appear in parallel, thereby exacerbating the stability problems. The analyses presented in the paper may be used to investigate such systems.

V. Conclusion

The paper explores the impact of two control strategies of LLC resonant converter – variable frequency control (VFC) and bang-bang charge control (BBCC) – on the stability margin of a cascaded converter system. In this respect, the analytic model of input impedance of VFC-based LLC resonant converter is derived using extended describing function (EDF) method. Further, the small-signal model of BBCC-based full-bridge LLC topology is derived, followed

by analytic representation of its open and closed-loop input impedance. The input impedance models in case of these two strategies are validated through impedance plots extracted from simulation. From the plots it is evident that the double pole resonance appearing in VFC-based converter can result in low stability margins, whereas its absence in BBCC-based converter should result in an improvement. Further, the developed models are applied to investigate the stability of a cascaded system comprising of a single-phase dual active bridge (DAB) converter feeding into a charge-controlled or frequency controlled LLC resonant converter. The frequency plots, from the model and simulation, of the minor-loop gain clearly indicate a marked improvement in system stability margins when BBCC-based LLC resonant converter is employed. The reported analyses are crucial in investigating the stability of systems where multiple LLC resonant point-of-load converters are fed from a source converter, for instance, in auxiliary power supply system of an automotive.

REFERENCES

[1] J. Deng, S. Li, S. Hu, C. C. Mi, and R. Ma, "Design methodology of llc resonant converters for electric vehicle battery chargers," *IEEE Transactions on Vehicular Technology*, vol. 63, no. 4, pp. 1581–1592, May 2014.

[2] S. Hu, J. Deng, C. Mi, and M. Zhang, "Optimal design of line level control resonant converters in plug-in hybrid electric vehicle battery chargers," *IET Electrical Systems in Transportation*, vol. 4, no. 1, pp. 21–28, March 2014.

[3] X. Zhang, X. Ruan, and C. K. Tse, "Impedance-based local stability criterion for dc distributed power systems," *IEEE Transactions on Circuits and Systems I: Regular Papers*, vol. 62, no. 3, pp. 916–925, March 2015.

[4] A. Khaligh, "Realization of parasitics in stability of dc-dc converters loaded by constant power loads in advanced multiconverter automotive systems," *IEEE Transactions on Industrial Electronics*, vol. 55, no. 6, pp. 2295–2305, June 2008.

[5] G. Pledl, M. Tauer, and D. Buecherl, "Theory of operation, design procedure and simulation of a bidirectional llc resonant converter for vehicular applications," in *2010 IEEE Vehicle Power and Propulsion Conference*, Sept 2010, pp. 1–5.

[6] S. Tian, F. C. Lee, and Q. Li, "Equivalent circuit modeling of LLC resonant converter," in *2016 IEEE Applied Power Electronics Conference and Exposition (APEC)*, Mar. 2016, pp. 1608–1615.

[7] Y. Yin, R. Zane, R. Erickson, and J. Glaser, "Direct modeling of envelope dynamics in resonant inverters," in *Power Electronics Specialist Conference, 2003. PESC '03. 2003 IEEE 34th Annual*, vol. 3, Jun. 2003, pp. 1313–1318 vol.3.

[8] S. R. Sanders, J. M. Noworolski, X. Z. Liu, and G. C. Verghese, "Generalized averaging method for power conversion circuits," in *, 21st Annual IEEE Power Electronics Specialists Conference, 1990. PESC '90 Record*, 1990, pp. 333–340.

[9] C. T. Rim and G. H. Cho, "Phasor transformation and its application to the DC/AC analyses of frequency phase-controlled series resonant converters (SRC)," *IEEE Transactions on Power Electronics*, vol. 5, no. 2, pp. 201–211, Apr. 1990.

[10] A. F. Witulski, A. F. Hernandez, and R. W. Erickson, "Small signal equivalent circuit modeling of resonant converters," *IEEE Transactions on Power Electronics*, vol. 6, no. 1, pp. 11–27, Jan. 1991.

[11] E. X. Yang, F. C. Lee, and M. M. Jovanovic, "Small-signal modeling of power electronic circuits by extended describing function concept," *Proc. Virginia Power Electronics Center Seminar*, pp. 167–178, 1991.

[12] Z. Hu, Y. F. Liu, and P. C. Sen, "Bang-bang charge control for llc resonant converters," *IEEE Transactions on Power Electronics*, vol. 30, no. 2, pp. 1093–1108, Feb 2015.

[13] D. Xiaoming and A. Q. Huang, "Current-mode variable-frequency control architecture for high-current low-voltage dc-dc converters," *IEEE Transactions on Power Electronics*, vol. 21, no. 4, pp. 1133–1137, July 2006.

[14] R. Beiranvand, B. Rashidian, M. R. Zolghadri, and S. M. H. Alavi, "Using llc resonant converter for designing wide-range voltage source," *IEEE Transactions on Industrial Electronics*, vol. 58, no. 5, pp. 1746–1756, May 2011.

[15] C. O. Yeon, J.-W. Kim, M.-H. Park, Y.-J. Jang, C.-Y. Lim, and G. W. Moon, "Bode plot and impedance asymptotes for light-load regulation of llc series resonant converter," in *2016 IEEE 8th International Power Electronics and Motion Control Conference (IPEMC-ECCE Asia)*, May 2016, pp. 3191–3197.

[16] R. Erickson and D. Maksimović, "Input Filter Design," in *Fundamentals of Power Electronics*, 2nd ed. New York: Kluwer, 2001, pp. 381–385.

[17] R. D. Middlebrook, "Input filter considerations in design and application of switching regulators," in *Conf. Rec. IEEE IAS Annu. Meeting*, 1979, pp. 366–382.

[18] H. Krishnamurthy and R. Ayyanar, "Stability analysis of cascaded converters for bidirectional power flow applications," in *INTELEC 2008 - 2008 IEEE 30th International Telecommunications Energy Conference*, Sept 2008, pp. 1–8.